VERSITA

Arch. Min. Sci., Vol. 57 (2012), No 4, p. 1101–1119

Electronic version (in color) of this paper is available: http://mining.archives.pl

DOI 10.2478/v10267-012-0073-7

MARIAN DOLIPSKI*, ERYK REMIORZ*, PIOTR SOBOTA*

DETERMINATION OF DYNAMIC LOADS OF SPROCKET DRUM TEETH AND SEATS BY MEANS OF A MATHEMATICAL MODEL OF THE LONGWALL CONVEYOR

WYZNACZENIE OBCIĄŻEŃ DYNAMICZNYCH ZĘBÓW I GNIAZD BĘBNA ŁAŃCUCHOWEGO ZA POMOCĄ MODELU MATEMATYCZNEGO PRZENOŚNIKA ŚCIANOWEGO

Scraper conveyors are one of the key machines forming part of mechanised longwall systems. They are currently the only means of transporting the mined rock from longwalls in hard coal mines. The hauling force caused by the drive is transmitted onto a link chain through drive wheels with their external shape corresponding to a geometric polygon. The number of teeth (seats) in such wheels ranges between 5 and 8. The horizontal links running on the drum are arranged in the drive wheel seats and are meshing with the teeth segments. The geometric relationships between the sprocket drum and the links are decisive for the position of the chain links in the seats. The abrasive wear of the chain parts and of the drive drum parts occurring due to conveyor operation is increasing the chain pitch and decreasing the wheel pitch. The position of a link in the seats changes as a result along with the load on the sprocket drum teeth and seats. Sprocket drums are the weakest element in longwall conveyors. It is, therefore, urgently necessary to determine the dynamic loads of such drums' teeth and seats. The article presents a physical model and a mathematical model of a longwall conveyor created for the purpose of determination of dynamic loads of the sprocket drum teeth and seats. The results of computer simulations are also presented (dynamic loads: in chains, dynamic loads of sprocket drums and dynamic loads of sprocket drums' teeth and seats) carried out using the created mathematical model for a 350 m long face conveyor.

Keywords: scraper conveyor, sprocket drum, mathematical and physical model, dynamic loads, teeth, seats

Koncentracja produkcji węgla kamiennego wymusza potrzebę prowadzenia intensywnych badań maszyn górniczych w aspekcie zwiększenia ich niezawodności i żywotności. Jedną z podstawowych maszyn wchodzących w skład ścianowych kompleksów zmechanizowanych są przenośniki zgrzebłowe. Przenośniki zgrzebłowe ścianowe są obecnie jedynymi środkami odstawy urobku z wyrobisk ścianowych w kopalniach węgla kamiennego. W czasie swojego rozwoju wyposażane były w różne typy łańcuchów pociągowych, z których najlepszym okazał się łańcuch ogniwowy. Przenośniki ścianowe mogą być wyposażone w jeden łańcuch, dwa łańcuchy skrajne, trzy łańcuchy lub dwa łańcuchy środkowe, przy czym ostatnie rozwiązanie stosowane jest najczęściej.

* INSTITUTE OF MINING MECHANISATION, FACULTY OF MINING AND GEOLOGY, SILESIAN UNIVERSITY OF TECHNOLOGY, AKADEMICKA 2, 44-100 GLIWICE, POLAND

Unauthenticated | 109.197.186.15
Download Date | 10/17/13 8:30 AM

Siła uciągu wywołana napędem przekazywana jest łańcuchowi poprzez koła napędowe, które mają postać geometryczną wieloboku i wyposażone są najczęściej w 5÷8 zębów (gniazd). Ogniwa poziome nabiegające na bęben układają się w gniazdach koła napędowego i wchodzą w zazębienie z segmentami zębów. O położeniu ogniw łańcucha w gniazdach decydują relacje geometryczne pomiędzy bębnem łańcuchowym a ogniwami. Zużycie ścierne elementów łańcucha i bębna napędowego następujące na skutek eksploatacji przenośnika powoduje zwiększenie podziałki łańcucha i zmniejszenie podziałki koła. W efekcie zmienia się zarówno położenie ogniw w gniazdach jak i obciążenie zębów i gniazd bębna łańcuchowego.

Obecnie najsłabszym elementem w przenośnikach ścianowych są bębny łańcuchowe. Zachodzi zatem pilna potrzeba poznania obciążeń dynamicznych zębów i gniazd tych bębnów.

Dla potrzeb wyznaczania obciążeń dynamicznych zębów i gniazd bębna łańcuchowego został rozbudowany model fizyczny i matematyczny przenośnika ścianowego o elementy zazębienia łańcuchowego. Dyskretny model fizyczny i matematyczny przenośnika ścianowego zbudowano wcześniej i wielokrotnie zweryfikowano go doświadczalnie. Po rozbudowaniu o elementy zazębienia łańcuchowego model fizyczny przyjmuje postać jak na rysunku 1. Ruch w tym rozbudowanym modelu fizycznym opisuje układ nieliniowych równań różniczkowych zwyczajnych drugiego rzędu (wzory 1, 2 i 3).

Podczas współdziałania bębna łańcuchowego o wymiarach normowych z łańcuchem o wydłużonej podziałce nabiegające ogniwo poziome nie styka się z dnem gniazda na całej swej długości. Ten wariant zazębienia charakteryzuje się tym, że ogniwa poziome łańcucha znajdujące się na kole gniazdowym o liczbie zębów z są nachylone względem den gniazd pod kątem ε tak, że ich torusy przednie stykają się dnami gniazd a torusy tylne stykają się z bokami roboczymi segmentów zębów koła o kącie pochylenia względem dna gniazda β. W celu jednoznacznego opisu położenia ogniw łańcucha w gniazdach koła wyznaczono parametry ε, u i α^u (rys. 2).

Przy analizowaniu współdziałania bębna łańcuchowego z łańcuchem ogniwowym uwzględniono zjawisko ruchliwości ogniw w przegubach podczas wzajemnego przechylania ogniw, którego następstwem jest przemieszczanie się punktu styku ogniw. Przechylaniu ogniwa poziomego względem ogniwa pionowego towarzyszy toczenie się ogniwa poziomego względem ogniwa pionowego w wyniku panującego w przegubie tarcia lub poślizg ogniw w przegubie w zależności od wartości modułu przegubu m^p i wartości współczynnika tarcia w przegubie μ^p. Podczas toczenia ogniwa poziomego w przegubie następuje przemieszczanie się punktu styku ogniw w przegubie, zaś podczas poślizgu ogniwa poziomego położenie punktu styku w przegubie ogniwa pionowego pozostaje bez zmian.

Ze względu na powtarzalność położenia ogniw w gniazdach koła łańcuchowego o liczbie zębów z podczas ich nabiegania następuje cykliczne obciążanie kolejnych den gniazd, flanek zębów i ogniw łańcucha siłami w czasie obrotu bębna łańcuchowego o kąt podziałowy $\varphi = 2\pi/z$. Podczas analizy obciążenia elementów bębna łańcuchowego przyjęto zmienność kąta obrotu bębna od chwili zetknięcia się torusa przedniego nabiegającego ogniwa poziomego z dnem gniazda ($\varphi = 0$) do chwili zetknięcia się torusa przedniego kolejnego ogniwa poziomego z dnem następnego gniazda ($\varphi = 2\pi/z$). W zakresie obrotu bębna łańcuchowego o kąt podziałowy wyróżniono trzy przedziały charakteryzujące się odmiennym sposobem obciążenia elementów bębna łańcuchowego (P1, P2 i P3 na rys. 1). Wzory od (4) do (39) opisują obciążenia dna gniazda i flanki zęba bębna łańcuchowego w tych przedziałach.

Utworzony model matematyczny pozwolił na komputerowe wyznaczenie obciążeń dynamicznych łańcuchów, bębnów napędowych oraz zębów i gniazd bębnów łańcuchowych w przenośniku ścianowym o długości 350 m (rys. 3÷8). W czasie badań symulowano stan nieluzowania łańcuchów i stan stałego luzowania.

Na podstawie przeprowadzonych badań komputerowych ruchu ustalonego ścianowego przenośnika zgrzebłowego, wyposażonego w bębny łańcuchowe o liczbie zębów $z = 8$, obciążonego urobkiem węglowym na całej długości sformułowano następujące wnioski:

1. Wydłużenie podziałki łańcucha, w praktyce spowodowane głównie zużyciem ściernym przegubów ogniw, powoduje osiadanie torusa tylnego ogniwa poziomego coraz wyżej na flance zęba (wzrost wartości kątów ε oraz α^u). Prowadzi to do skracania czasu od chwili zetknięcia się torusa przedniego ogniwa poziomego z dnem gniazda do chwili zetknięcia się torusa tylnego tego ogniwa z flanką zęba. Konsekwencją tego jest zmniejszanie się wartości maksymalnej obciążenia dna gniazda w punkcie styku z torusem przednim ogniwa oraz wzrost maksymalnej wartości wymaganej siły tarcia zapobiegającej poślizgowi torusa tylnego po flance zęba zarówno w stanie stałego luzowania jak i w stanie nieluzowania łańcucha.
2. Stosunek maksymalnej wartości siły obciążającej flankę zęba w punkcie styku z torusem tylnym ogniwa do maksymalnej wartości siły obciążającej dno gniazda w punkcie styku z torusem przednim

Unauthenticated | 109.197.186.15
Download Date | 10/17/13 8:30 AM

ogniwa oraz stosunek maksymalnej wartości wymaganej siły tarcia zapobiegającej poślizgowi torusa tylnego po flance zęba do maksymalnej wartości siły obciążającej dno gniazda w punkcie styku z torusem przednim ogniwa rosną nieliniowo ze wzrostem wydłużenia podziałki ogniw. Wzrosty te przebiegają niemal identycznie dla stanu stałego luzowania i stanu nieluzowania łańcucha.

3. Zwiększenie podziałki łańcucha od 1% do 4% spowodowało ponad czterokrotny wzrost wartości maksymalnej siły tarcia zapobiegającej poślizgowi torusa tylnego ogniwa poziomego po flance zęba w stronę dna gniazda. Jeżeli wartość siły tarcia rozwiniętego wywołanego siłą nacisku torusa tylnego ogniwa poziomego na flankę zęba jest co najmniej równa wartości rozpatrywanej siły tarcia to układ sił jest w równowadze. Jeśli natomiast siła tarcia pochodząca od nacisku torusa tylnego na flankę zęba jest mniejsza od wartości tej siły tarcia to następuje poślizg torusa tylnego po flance zęba w stronę dna gniazda. Z tego względu duże wartości rozważanej siły tarcia w miejscu styku torusa tylnego ogniwa poziomego z flanką zęba są niekorzystne, gdyż zwiększają możliwość wystąpienia poślizgu ogniwa po flance zęba co powoduje zwiększenie zużycia ściernego flanki zęba obniżając trwałość bębna łańcuchowego i powodując zmniejszenie sprawności zazębienia łańcuchowego.

Słowa kluczowe: przenośnik ścianowy, bęben łańcuchowy, model fizyczny i matematyczny, obciążenia dynamiczne zębów, obciążenia dynamiczne gniazd

1. Introduction

The concentration of hard coal production necessitates the intensive tests of mining machines in the context of improving their reliability and life (Dolipski, 1997; Hoseinie et al., 2011; Krauze et al., 2009; Krauze, 2004; Langosch & Ruppel, 2008). Scraper conveyors are one of the key machines forming part of mechanised longwall systems.

Longwall scraper conveyors are currently the only means of transporting the mined rock from longwalls in hard coal mines. The conveyors, throughout their development, have been equipped with the different types of drive chains, with a link chain turning out to be the best. Its essential advantages include simple production technology, the links can be rotated relatively in the horizontal and vertical plane, high tensile strength, easy installation and the simple and fast linking of the broken sections using connecting links. A mining plain link chain consists of alternate horizontal (active) and vertical (passive) links. The chains are made of a steel rod with the d diameter and are shaped as flat rings with a front torus, rear torus and two drums.

The hauling force caused by the drive is transmitted onto a link chain through drive wheels with their external shape corresponding to a geometric polygon. The number of teeth (seats) in such wheels ranges between 5 and 8. The horizontal links running on the drum are arranged in the drive wheel seats and are meshing with the teeth segments. The geometric relationships between the sprocket drum and the links are decisive for the position of the chain links in the seats. The abrasive wear of the chain parts and of the drive drum parts occurring due to conveyor operation is increasing the chain pitch and decreasing the wheel pitch. As a result the position of links in the seats changes along with the load on the sprocket drum teeth and seats.

Investigations into sprocket drums have been concentrated to date on the meshing geometry and on the calculation of static loads (Dolipski, 1997; Strümpfel, 1989; Uhr, 1993), and the investigations aimed at determining dynamic loads in longwall conveyors were concentrated on chains and couplings (Dolipski, 1997, 2001; Kallrath & Brychta, 1986; Wölfe & Flöte, 2000; Ziegler et al., 2007). Sprocket drums are currently the weakest element in longwall conveyors. It is, therefore, urgently necessary to determine the dynamic loads of such drums' teeth and seats.

Unauthenticated | 109.197.186.15
Download Date | 10/17/13 8:30 AM

2. Discrete physical and mathematical model

High-capacity longwall scraper conveyors with two central chains are used most often these days in longwall faces. The hauling force caused by the drive is transmitted onto a scraper chain by means of a sprocket drum equipped with two seat wheels. A physical and mathematical longwall conveyor model has been extended with the chain meshing elements for the purpose of dynamic loads determination of the sprocket drum teeth and seats. A discrete physical and mathematical longwall conveyor model was built earlier (Dolipski, 1997) and verified experimentally many times. The physical model, after expanding it with the chain meshing elements, assumes its form as in Fig. 1. Motion in this expanded physical model is described with the following system of ordinary nonlinear second-order differential equations:

$$m_{1\kappa 1}\cdot\ddot{q}_{1\kappa 1}+Z_{1\kappa 1}\cdot H[\ ]\cdot\left[k_{1\kappa B}\cdot(q_{1\kappa 1}-\varphi_B\cdot R_{0\kappa B})+h_{1\kappa B}\cdot(\dot{q}_{1\kappa 1}-\dot{\varphi}_B\cdot R_{0\kappa B})+S_{1\kappa 1}\right]+$$
$$-Z_{1\kappa 2}\cdot H[\ ]\cdot\left[k_{1\kappa 1}\cdot(q_{1\kappa 2}-q_{1\kappa 1})+h_{1\kappa 1}\cdot(\dot{q}_{1\kappa 2}-\dot{q}_{1\kappa 1})+S_{1\kappa 1}\right]+W_{1\kappa 1}=0$$

.....

$$m_{1\kappa i}\cdot\ddot{q}_{1\kappa i}+Z_{1\kappa i}\cdot H[\ ]\cdot\left[k_{1\kappa(i-1)}\cdot(q_{1\kappa i}-q_{1\kappa(i-1)})+h_{1\kappa(i-1)}\cdot(\dot{q}_{1\kappa i}-\dot{q}_{1\kappa(i-1)})+S_{1\kappa i}\right]+$$
$$-Z_{1\kappa(i+1)}\cdot H[\ ]\cdot\left[k_{1\kappa i}\cdot(q_{1\kappa(i+1)}-q_{1\kappa i})+h_{1\kappa i}\cdot(\dot{q}_{1\kappa(i+1)}-\dot{q}_{1\kappa i})+S_{1\kappa i}\right]+W_{1\kappa i}=0$$

.....

$$m_{1\kappa j}\cdot\ddot{q}_{1\kappa j}+Z_{1\kappa j}\cdot H[\ ]\cdot\left[k_{1\kappa(j-1)}\cdot(q_{1\kappa j}-q_{1\kappa(j-1)})+h_{1\kappa(j-1)}\cdot(\dot{q}_{1\kappa j}-\dot{q}_{1\kappa(j-1)})+S_{1\kappa j}\right]+$$
$$-Z_{1\kappa A}\cdot H[\ ]\cdot\left[k_{1\kappa A}\cdot(\varphi_A\cdot R_{0\kappa A}-q_{1\kappa j})+h_{1\kappa A}\cdot(\dot{\varphi}_A\cdot R_{0\kappa A}-\dot{q}_{1\kappa j})+S_{1\kappa j}\right]+W_{1\kappa j}=0$$

$$I_A\cdot\dot{\varphi}_A+Z_{11A}\cdot H[\ ]\cdot\left[S^H_{11A}\right]\cdot R_{11A}+Z_{12A}\cdot H[\ ]\cdot\left[S^H_{12A}\right]\cdot R_{12A}+$$
$$-Z_{211}\cdot H[\ ]\cdot\left[k_{21A}(q_{211}-\varphi_A\cdot R_{01A})+h_{21A}\cdot(\dot{q}_{211}-\dot{\varphi}_A\cdot R_{01A})+S_{21A}\right]\cdot R_{21A}+$$
$$-Z_{221}\cdot H[\ ]\cdot\left[k_{22A}\cdot(q_{221}-\varphi_A\cdot R_{02A})+h_{22A}\cdot(\dot{q}_{221}-\dot{\varphi}_A\cdot R_{02A})+S_{22A}\right]\cdot R_{22A}=$$
$$k_{A1}\cdot(\varphi_{A1}-\varphi_A)+h_{A1}\cdot(\dot{\varphi}_{A1}-\dot{\varphi}_A)+Z_{11A}\cdot S_{11A}\cdot R_{11A}+Z_{12A}\cdot S_{12A}\cdot R_{12A}+$$
$$-Z_{21A}\cdot H[\ ]\cdot[S_{21A}]\cdot R_{21A}-Z_{22A}\cdot H[\ ]\cdot[S_{22A}]\cdot R_{22A}$$

$$I_{A1}\cdot\ddot{\varphi}_{A1}+k_{A1}\cdot(\varphi_{A1}-\varphi_A)+h_{A1}\cdot(\dot{\varphi}_{A1}-\dot{\varphi}_A)+k_{A2}\cdot(\varphi_{A1}-\varphi_{A2})+h_{A2}\cdot(\dot{\varphi}_{A1}-\dot{\varphi}_{A2})+Z_{11A}\cdot S_{11A}\cdot R_{11A}$$
$$+Z_{12A}\cdot S_{12A}\cdot R_{12A}-Z_{21A}\cdot H[\ ]\cdot[S_{21A}]\cdot R_{21A}-Z_{22A}\cdot H[\ ]\cdot[S_{22A}]\cdot R_{22A}=0$$

.....

$$I_{A4}\cdot\ddot{\varphi}_{A4}+k_{A4}\cdot(\varphi_{A4}-\varphi_{A3})+h_{A4}\cdot(\dot{\varphi}_{A4}-\dot{\varphi}_{A3})+Z_{11A}\cdot S_{11A}\cdot R_{11A}+Z_{12A}\cdot S_{12A}\cdot R_{12A}+$$
$$-Z_{21A}\cdot H[\ ]\cdot[S_{21A}]\cdot R_{21A}-Z_{22A}\cdot H[\ ]\cdot[S_{22A}]\cdot R_{22A}=M_A$$

Unauthenticated | 109.197.186.15
Download Date | 10/17/13 8:30 AM

$$m_{2\kappa 1}\cdot\ddot{q}_{1\kappa 1}+Z_{2\kappa 1}\cdot H[\ ]\cdot\left[k_{2\kappa A}\cdot(q_{2\kappa 1}-\varphi_A\cdot R_{0\kappa A})+h_{2\kappa A}\cdot(\dot{q}_{2\kappa 1}-\dot{\varphi}_A\cdot R_{0\kappa A})+S_{2\kappa 1}\right]+$$
$$-Z_{2\kappa 2}\cdot H[\ ]\cdot\left[k_{2\kappa 1}\cdot(q_{2\kappa 2}-q_{2\kappa 1})+h_{2\kappa 1}\cdot(\dot{q}_{2\kappa 2}-\dot{q}_{2\kappa 1})+S_{2\kappa 1}\right]+W_{2\kappa 1}=0$$

.....

$$m_{2\kappa i}\cdot\ddot{q}_{2\kappa i}+Z_{2\kappa i}\cdot H[\ ]\cdot\left[k_{2\kappa(i-1)}\cdot(q_{2\kappa i}-q_{2\kappa(i-1)})+h_{2\kappa(i-1)}\cdot(\dot{q}_{2\kappa i}-\dot{q}_{2\kappa(i-1)})+S_{2\kappa i}\right]+$$
$$-Z_{2\kappa(i+1)}\cdot H[\ ]\cdot\left[k_{2\kappa i}\cdot(q_{2\kappa(i+1)}-q_{2\kappa i})+h_{2\kappa i}\cdot(\dot{q}_{2\kappa(i+1)}-\dot{q}_{2\kappa i})+S_{2\kappa i}\right]+W_{2\kappa i}=0$$

.....

$$m_{2\kappa j}\cdot\ddot{q}_{2\kappa j}+Z_{2\kappa j}\cdot H[\ ]\cdot\left[k_{2\kappa(j-1)}\cdot(q_{2\kappa j}-q_{2\kappa(j-1)})+h_{2\kappa(j-1)}\cdot(\dot{q}_{2\kappa j}-\dot{q}_{2\kappa(j-1)})+S_{2\kappa j}\right]+$$
$$-Z_{2\kappa B}\cdot H[\ ]\cdot\left[k_{2\kappa B}\cdot(\varphi_B\cdot R_{0\kappa B}-q_{2\kappa j})+h_{2\kappa B}\cdot(\dot{\varphi}_B\cdot R_{0\kappa B}-\dot{q}_{2\kappa j})+S_{2\kappa j}\right]+W_{2\kappa j}=0$$

$$I_B\cdot\ddot{\varphi}_B+Z_{21B}\cdot H[\ ]\cdot\left[S^H_{21B}\right]\cdot R_{21B}+Z_{22B}\cdot H[\ ]\cdot\left[S^H_{22B}\right]\cdot R_{22B}+$$
$$-Z_{111}\cdot H[\ ]\cdot\left[k_{11B}\cdot(q_{111}-\varphi_B\cdot R_{01B})+h_{11B}\cdot(\dot{q}_{111}-\dot{\varphi}_B\cdot R_{01B})+S_{11B}\right]\cdot R_{11B}+$$
$$-Z_{121}\cdot H[\ ]\cdot\left[k_{12B}\cdot(q_{121}-\varphi_B\cdot R_{02B})+h_{12B}\cdot(\dot{q}_{121}-\dot{\varphi}_B\cdot R_{02B})+S_{12B}\right]\cdot R_{12B}=$$
$$k_{B1}\cdot(\varphi_{B1}-\varphi_B)+h_{B1}\cdot(\dot{\varphi}_{B1}-\dot{\varphi}_B)+Z_{21B}\cdot S_{21B}\cdot R_{21B}+Z_{22B}\cdot S_{22B}\cdot R_{22B}+$$
$$-Z_{11B}\cdot H[\ ]\cdot[S_{11B}]\cdot R_{11B}-Z_{12B}\cdot H[\ ]\cdot[S_{12B}]\cdot R_{12B}$$

$$I_{B1}\cdot\dot{\varphi}_{B1}+k_{B1}\cdot(\varphi_{B1}-\varphi_B)+h_{B1}\cdot(\dot{\varphi}_{B1}-\dot{\varphi}_B)+k_{B2}\cdot(\varphi_{B1}-\varphi_{B2})+h_{B2}\cdot(\dot{\varphi}_{B1}-\dot{\varphi}_{B2})+Z_{11B}\cdot S_{11B}\cdot R_{11B}$$
$$+Z_{12B}\cdot S_{12B}\cdot R_{12B}-Z_{21B}\cdot H[\ ]\cdot[S_{21B}]\cdot R_{21B}-Z_{22B}\cdot H[\ ]\cdot[S_{22B}]\cdot R_{22B}=0$$

.....

$$I_{B4}\cdot\dot{\varphi}_{B4}+k_{B4}\cdot(\varphi_{B4}-\varphi_{B3})+h_{B4}\cdot(\dot{\varphi}_{B4}-\dot{\varphi}_{B3})+Z_{21B}\cdot S_{21B}\cdot R_{21B}+Z_{22B}\cdot S_{22B}\cdot R_{22B}+$$
$$-Z_{11B}\cdot H[\ ]\cdot[S_{11B}]\cdot R_{11B}-Z_{12B}\cdot H[\ ]\cdot[S_{12B}]\cdot R_{12B}=M_B \tag{1}$$

whereas:

$$S^H_{1\kappa A}=k_{1\kappa A}\cdot(\varphi_A\cdot R_{0\kappa A}-q_{1\kappa j})+h_{1\kappa A}(\dot{\varphi}_A\cdot R_{0\kappa A}-\dot{q}_{1\kappa j})+S_{1\kappa A} \tag{2}$$

$$S^H_{2\kappa B}=k_{2\kappa B}\cdot(\varphi_B\cdot R_{0\kappa B}-q_{2\kappa j})+h_{2\kappa B}\cdot(\dot{\varphi}_B\cdot R_{0\kappa B}-\dot{q}_{2\kappa j})+S_{2\kappa B} \tag{3}$$

$$i=2,\ 3,\ \ldots,\ j-1$$

$$\kappa=1,\ 2$$

where:

h — a substitute damping coefficient of additional longitudinal chain dampers,

h_{A1}, h_{B1} — a substitute damping coefficient of sprocket drum in the main drive (index A) and auxiliary drive (index B),

Unauthenticated | 109.197.186.15
Download Date | 10/17/13 8:30 AM

h_{A2}, h_{B2} — a substitute damping coefficient of reducer in the main drive (index A) and auxiliary drive (index B),
h_{A3}, h_{B3} — a substitute damping coefficient of coupling in the main drive (index A) and auxiliary drive (index B),
h_{A4}, h_{B4} — a substitute damping coefficient of the driving motor in the main drive (index A) and auxiliary drive (index B),
$H[\ ]$ — Heaviside's function (square bracket means the content of the Heaviside's function argument),
I_A, I_B — moment of inertia of sprocket drum in the main drive (index A) and auxiliary drive (index B),
I_{A1}, I_{B1} — moment of inertia of reducer reduced onto the sprocket drum shaft in the main and auxiliary drive,
I_{A2}, I_{B2} — moment of inertia of the output member of the coupling reduced onto the sprocket drum shaft in the main and auxiliary drive,
I_{A3}, I_{B3} — moment of inertia of the input member of the coupling reduced onto the sprocket drum shaft in the main and auxiliary drive,
$\mathrm{I_{A4}}$, I_{B4} — moment of inertia of the motor rotor reduced onto the sprocket drum shaft in the main and auxiliary drive,
k — specific rigidity of the chain's flexible bond,
k_{A1}, k_{B1} — specific torsional rigidity of the drive drum reduced onto the sprocket drum shaft in the main drive (A) and auxiliary drive (B),
k_{A2}, k_{B2} — specific torsional rigidity of the reducer reduced onto the sprocket drum shaft in the main drive (A) and auxiliary drive (B),
k_{A3}, k_{B3} — specific torsional rigidity of the coupling reduced onto the sprocket drum shaft in the main drive (A) and auxiliary drive (B),
k_{A4}, k_{B4} — specific torsional rigidity of the asynchronous motor rotor reduced onto the sprocket drum shaft in the main drive (A) and auxiliary drive (B),
m — substitute vibrating mass,
$\mathrm{M_A}$, M_B — driving torque of the asynchronous motor in the main and auxiliary drive reduced onto the sprocket drum shaft,
q — translation coordinates,
R_{11A}, R_{12A} — functions of radiuses of the chain No. 1 and No. 2 running on the sprocket drum of the main drive,
R_{21B}, R_{22B} — functions of radiuses of the chain No. 1 and No. 2 running on the sprocket drum of the auxiliary drive,
R_{21A}, R_{22A} — functions of radiuses of the chain No. 1 and No. 2 running off the sprocket drum of the main drive,
R_{11B}, R_{12B} — functions of radiuses of the chain No. 1 and No. 2 running off the sprocket drum of the auxiliary drive,
R_{01A}, R_{02A} — pitch radiuses of sprocket wheels of the drive A,
R_{01B}, R_{02B} — pitch radiuses of sprocket wheels of the drive B,
S — static load in the chain (being the function of resistance of motion, residual initial chain tension and power distribution factor),
W — force of external friction in the place of arranging the substitute vibrating mass,

Unauthenticated | 109.197.186.15
Download Date | 10/17/13 8:30 AM

Z — the chain break coefficient ($Z = 0$ for broken chain, $Z = 1$ if chain breakage does not occur),
φ — rotation coordinates.

When a sprocket drum with standard dimensions is co-working with a chain with the elongated pitch, the running-on horizontal link does not contact the seat bottom along its entire length. This meshing variant is characterised by the fact that the horizontal chain links located on the seat wheel with the number of teeth z are inclined relative to the seat bottoms under the angle ε so that their front tori contact the seat bottoms and the rear tori contact the working sides of the wheel teeth segments with the inclination angle relative to the seat bottom β. The following parameters are determined in order to clearly describe the location of the chain links in the wheel seats (Fig. 2) (Dolipski et al., 2010):

- the links' inclination angle relative to the bottoms of the wheel seats ε;
- the distance between the centre of the joint with the front torus of the horizontal link from the beginning of the side of a regular polygon u;
- the rotation angle of the vertical link relative to the preceding horizontal link in the middle of the joint with the horizontal link rear torus α^u.

The longer relative elongation of the pitch the greater values are achieved by the parameters describing the location of links in the sprocket wheel seats (ε, u and α^u).

The mobility effect of links in joints, when the links are tilting mutually, has been considered when analysing the co-working of the sprocket drum with the link chain, the result of which is the displacement of the contact point of the links. The tilting of the horizontal link relative to the vertical link is accompanied by the rolling of the horizontal link relative to the vertical link as a result of the friction existing in the joint or by the slip of links in the joint depending on the value of the joint module m^p and the value of the friction coefficient in the joint μ^p. When the horizontal link is rolling, the contact point of the links is displacing in the joint, and the position of the contact point in the vertical link joint remains unchanged during the slip of the horizontal link.

Due to the repeatability of the links' location in the sprocket wheel seats with the number of teeth z, when the teeth are running on, the relevant seats bottoms, teeth flanks and chain links are loaded with forces in a cyclic manner when the sprocket drum is rotated by the pitch angle of $\varphi = 2\pi/z$. It was assumed when analysing the loading of the sprocket drum elements that the drum rotation angle is changing from the moment the front torus of the running-on horizontal link is contacting the seat bottom ($\varphi = 0$) until the front torus of another horizontal link is contacting the bottom of the next seat ($\varphi = 2\pi/z$). Three ranges, characterised by the different loading of the sprocket drum parts, are differentiated for sprocket drum rotation by the pitch angle.

The first range (P1 in Fig. 1) lasts from the moment the front torus of the horizontal link contacts the seat bottom until the rear torus of the horizontal link contacts the tooth flank and includes drum rotation by the angle φ changing within the range of:

$$0 \le \varphi \le \frac{2 \cdot \pi}{z} - \alpha^u + \lambda \tag{4}$$

The horizontal link that is meshed is loaded with the run-on force S^H (determined with the formula (2) and the system of equations (1) in the main drive and with the formula (3) and the system of equations (1) in the auxiliary drive), with the reactive force N between the front torus of the horizontal link and the seat bottom, whereas the slip of the front torus on the seat bottom

Unauthenticated | 109.197.186.15
Download Date | 10/17/13 8:30 AM

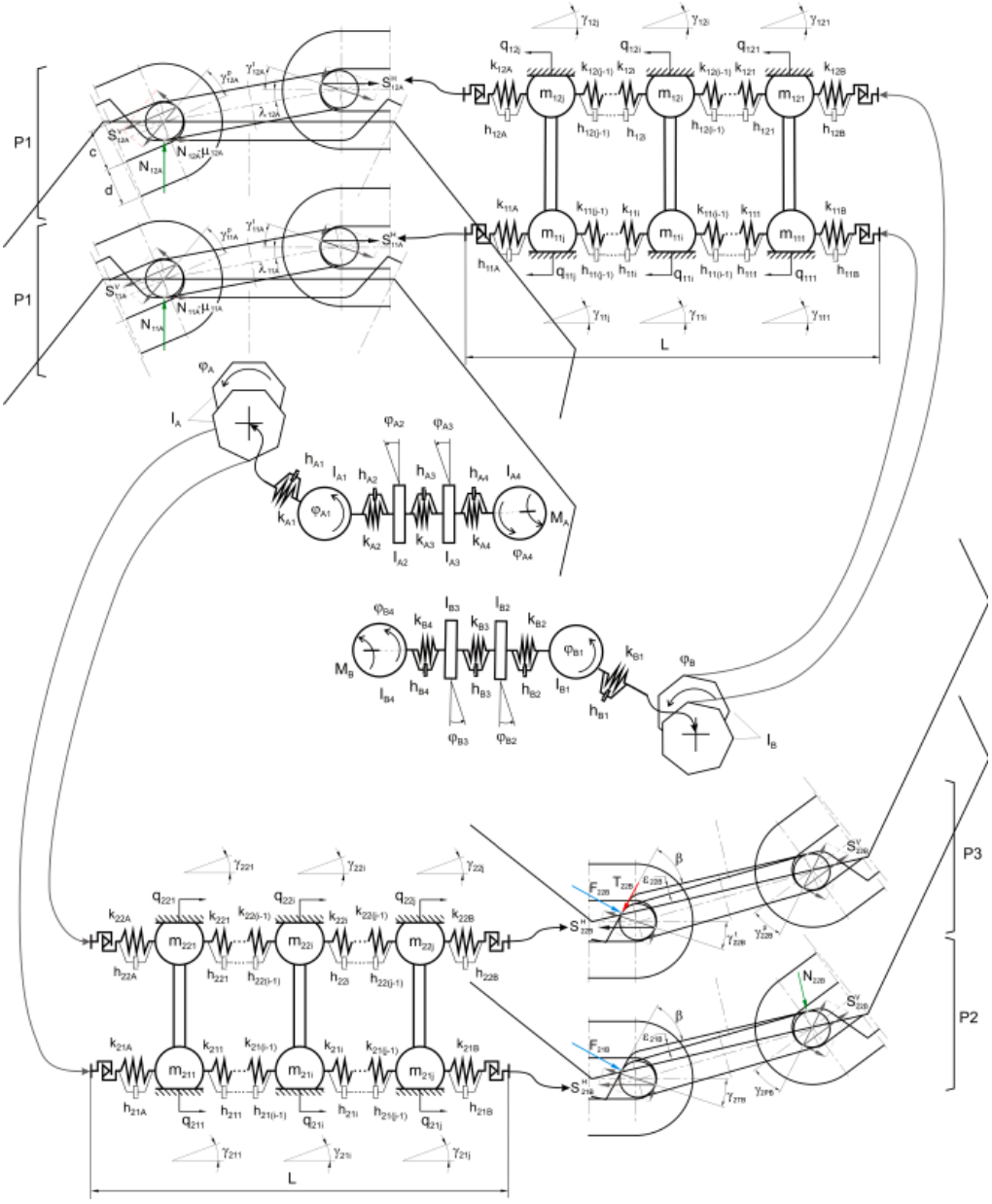

Fig. 1. Physical model of a longwall scraper conveyor with the sprocket drums marked

is accompanied by the friction force, perpendicular to the reaction, dependent upon the value of reaction and friction coefficient on the seat bottom μ^g and the force S^V transmitted from the horizontal link on the preceding vertical link (P1 in Fig. 1). The tilting of the horizontal link relative

Unauthenticated | 109.197.186.15
Download Date | 10/17/13 8:30 AM

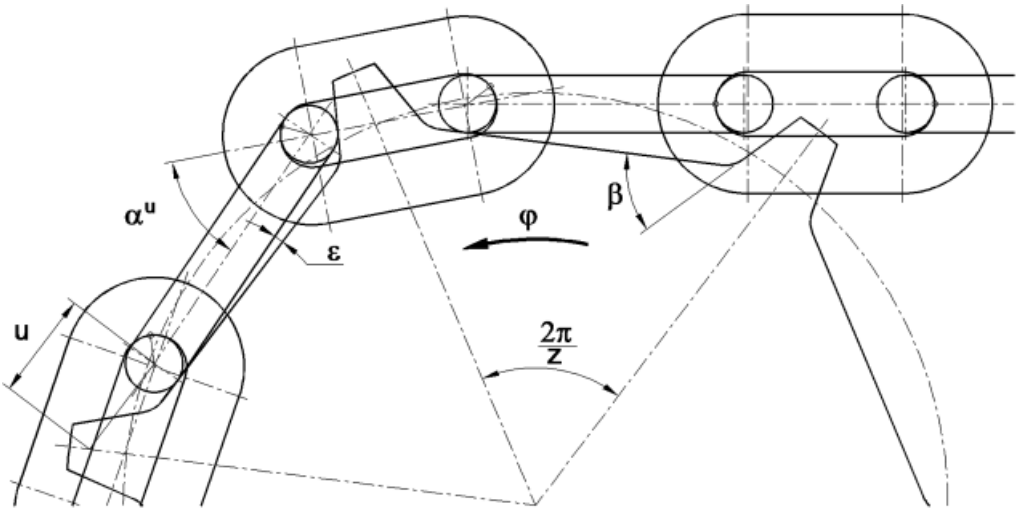

Fig. 2. Location of chain links in the sprocket wheel seats

to the preceding vertical link is accompanied by link rolling or slip in the joint resulting in the displacement of the contact point of the links by the angle γ^p. The mobility of links in the joint of the horizontal link and of the preceding vertical link, and the friction force at the seat bottom are forcing the tilting of the running-on vertical link from the axis of the meshing horizontal link by the deflection angle of λ and this is accompanied by the rolling or slip of the link in the joint causing the displacement of the contact point of the links by the angle γ^t.

The equations of balances of forces acting on the horizontal link are then assuming the following form:

$$S^H \cdot \cos(\nu - \varphi) - S^V \cdot \cos(\nu) + N \cdot \mu^g = 0 \tag{5}$$

$$S_H \cdot \sin(\nu - \varphi) - S_V \cdot \sin(\nu) + N \tag{6}$$

$$S^V \cdot \frac{d}{2} \cdot \sin(\gamma^p) + N \cdot \mu^g \cdot \frac{d}{2} - S^H \cdot \left[(p+d) \cdot \sin(\lambda) + \frac{d}{2} \cdot \sin(\gamma^t) \right] = 0 \tag{7}$$

where:

$$\nu = \frac{2 \cdot \pi}{z} + \varepsilon^n - \alpha^u \tag{8}$$

The forces S^V and N in the function of the run-on force S^H can be determined from the equations recorded with the relationships (5) and (6):

$$\frac{S^V}{S^H} = \frac{\cos(\nu - \varphi) - \mu^g \cdot \sin(\nu - \varphi)}{\cos(\nu) - \mu^g \cdot \sin(\nu)} \tag{9}$$

Unauthenticated | 109.197.186.15
Download Date | 10/17/13 8:30 AM

$$\frac{N}{S^H} = \frac{\sin(\varphi)}{\cos(\nu) - \mu^g \cdot \sin(\nu)} \tag{10}$$

and the deviation angle λ can be determined from the equation (7) according to the mobility of links in the joint. Links are rolling for the following range of the angle of rotation:

$$0 \le (\varphi - \lambda) \le \varphi^{gr} \tag{11}$$

whereas:

$$\varphi^{gr} = \frac{(1 - m^p)}{m^p} \cdot \arctan(\mu^p) \tag{12}$$

$$\gamma^p = \frac{m^p}{(1 - m^p)} \cdot (\varphi - \lambda) \tag{13}$$

The slip of links in the joint occur for the following range of the angle of rotation:

$$\varphi^{gr} \le \varphi \le \frac{2 \cdot \pi}{z} - \alpha^u + \lambda \tag{14}$$

whereas:

$$\gamma^p = \arctan(\mu^p) \tag{15}$$

Similarly, the mobility range of the deviation angle of the vertical link in the axis of the horizontal link λ should consider the rolling or slip of links in the joint. Links are rolling for the following range:

$$0 \le \lambda \le \lambda^{gr} \tag{16}$$

whereas:

$$\lambda^{gr} = \frac{(1 - m^p)}{m^p} \cdot \arctan(\mu^p) \tag{17}$$

$$\gamma^t = \frac{m^p}{(1 - m^p)} \cdot \lambda \tag{18}$$

meanwhile the slip of links in the joint occur for the following angle of rotation:

$$\lambda > \lambda^{gr} \tag{19}$$

whereas:

$$\gamma^t = \arctan(\mu^p) \tag{20}$$

Unauthenticated | 109.197.186.15
Download Date | 10/17/13 8:30 AM

The second range (P2 in Fig. 1) lasts from the moment the rear torus of the horizontal torus contacts the tooth flank until the reaction N reaches a zero value and includes drum rotation by the angle φ changing within the following range:

$$\frac{2\cdot\pi}{z} - \alpha^u + \lambda \le \varphi \le \varphi^{N0} \tag{21}$$

A horizontal link is loaded with the run-on force S^H, with the force of reaction N between the front torus of the horizontal link and the seat bottom, with the force of reaction F in the contact point of the rear torus of the horizontal link with the tooth flank and with the force S^V transmitted from the horizontal link onto the preceding vertical link (P2 in fig. 1). The equations of balances of forces acting on the horizontal link are then assuming the following form:

$$S^H \cdot \cos(\varphi - \nu) - S^V \cdot \cos(\nu) - F \cdot \sin(\beta) = 0 \tag{22}$$

$$-S^H \cdot \sin(\varphi - \nu) - S^V \cdot \sin(\nu) + F \cdot \cos(\beta) + N = 0 \tag{23}$$

$$S^H \cdot \left[(p+d) \cdot \sin(\varphi - \nu + \varepsilon^n) + \frac{d}{2} \cdot \sin(\gamma^t) \right] - S^V \cdot \frac{d}{2} \cdot \sin(\gamma^p) - F \cdot (p+d) \cdot \cos(\beta - \varepsilon^n) = 0 \tag{24}$$

The forces S^V, F and N in the function of the run-on force S^H can be determined from the equation notated with the relationships (22), (23) and (24):

$$\frac{S^V}{S^H} = \frac{\left[2 \cdot (p+d) \cdot \sin(\varphi - \nu + \varepsilon^n) + d \cdot \sin(\gamma^t) \right] \cdot \sin(\beta) - 2 \cdot (p+d) \cdot \cos(\varphi - \nu) \cdot \cos(\beta - \varepsilon^n)}{d \cdot \sin(\beta) \cdot \sin(\gamma^p) - 2 \cdot (p+d) \cdot \cos(\beta - \varepsilon^n) \cdot \cos(\nu)} \tag{25}$$

$$\frac{F}{S^H} = \frac{\cos(\varphi - \nu)}{\sin(\beta)} - \frac{S^V}{S^H} \cdot \frac{\cos(\nu)}{\sin(\beta)} \tag{26}$$

$$\frac{N}{S^H} = \sin(\varphi - \nu) + \frac{S^V}{S^H} \cdot \sin(\nu) - \frac{F}{S^H} \cdot \cos(\beta) \tag{27}$$

The variability range of the vertical link rotation angle relative to the preceding horizontal link has to take into account either the rolling of the vertical link relative to the horizontal link as a result of the friction existing in the joint or the slip of links in the joint. Links' rolling occurs already before contacting the rear torus of the horizontal link within the range of the angle of rotation λ and lasts until the limit angle is reached φ^{gr}, whereas

$$\varphi^{gr} = \frac{(1 - m^p)}{m^p} \cdot \arctan(\mu^p) + \frac{2 \cdot \pi}{z} - \alpha^u \tag{28}$$

$$\gamma^t = \frac{m^p}{(1 - m^p)} \cdot \left(\varphi - \frac{2 \cdot \pi}{z} + \alpha^u \right) \tag{29}$$

Unauthenticated | 109.197.186.15
Download Date | 10/17/13 8:30 AM

The slip of links in the joint occurs for the following range of the angle of rotation:

$$\varphi^{gr} \le \varphi \le \frac{2 \cdot \pi}{z} \tag{30}$$

whereas:

$$\gamma^t = \arctan(\mu^p) \tag{31}$$

As the value of the drum rotation angle φ is rising so is decreasing the values of the force in the preceding vertical link S^V and of the reaction between the front torus of the link and the bottom of the seat N while the value of the reaction between the rear torus of the horizontal link and the tooth flank F is rising. The values of forces up to the rotation angle φ^{N0} at which the value of reaction N falls to zero have been determined from the above dependencies. The third range (P3 in Fig. 1) starts from this moment lasting from the time the reaction N reaches a zero value until the front torus contacts the next horizontal link with the bottom of the next seat:

$$\varphi^{N0} \le \varphi \le \frac{2 \cdot \pi}{z} \tag{32}$$

The system of forces acting on the horizontal link changes for the angle $\varphi > \varphi^{N0}$ and the force T occurs on the tooth flank necessary for maintaining the balance of the horizontal link preventing the slip of the rear torus of the horizontal link towards the seat bottom at the tooth flank (P3 in Fig. 1). Equations for the balance of the horizontal link are then assuming the following form:

$$S^H \cdot \cos(\varphi - \nu) - S^V \cdot \cos(\nu) - F \cdot \sin(\beta) + T \cdot \cos(\beta) = 0 \tag{33}$$

$$-S^H \cdot \sin(\varphi - \nu) - S^V \cdot \sin(\nu) + F \cdot \cos(\beta) + T \cdot \sin(\beta) = 0 \tag{34}$$

$$-S^V \cdot \left[(p + d) \cdot \sin(\nu - \varepsilon^n) + \frac{d}{2} \cdot \sin(\gamma^p) \right] + S^H \cdot \frac{d}{2} \cdot \sin(\gamma^t) - T \cdot \frac{d}{2} = 0 \tag{35}$$

The forces S^V, F and T as the function of the run-on force S^H can be determined from the equation notated with the relationships (33), (34) and (35):

$$\frac{T}{S^H} = \frac{S^V}{S^H} \cdot \cos(\beta - \nu) - \cos(\beta - \nu + \varphi) \tag{36}$$

$$\frac{T}{S^H} = \frac{S^V}{S^H} \cdot \cos(\beta - \nu) - \cos(\beta - \nu + \varphi) \tag{37}$$

$$\frac{F}{S^H} = \frac{\cos(\varphi - \nu)}{\sin(\beta)} - \frac{S^V}{S^H} \cdot \frac{\cos(\nu)}{\sin(\beta)} + \frac{T}{S^H} \cdot \frac{1}{\tan(\beta)} \tag{38}$$

Unauthenticated | 109.197.186.15
Download Date | 10/17/13 8:30 AM

If the reaction N does not reach the zero value in the second range until the moment the front torus of the next horizontal link contacts the bottom of the next seat, i.e. for:

$$\varphi^{N0} \geq \frac{2 \cdot \pi}{z} \tag{39}$$

then the third range of loading the sprocket drum elements does not occur.

3. Computer tests

A longwall scraper conveyor with the length of L = 350 m equipped with a single main drive and a single auxiliary drive was subjected to computer tests. The driving systems with asynchronous motors with the power of 400 kW each were equipped with sprocket drums with the number of teeth of z = 8 and the pitch angle of 45°. The drums were co-working with two central chains sized 34 × 126 with the joint module of m^p = 0,85. The upper conveyor branch was loaded with the mined coal with the intensity of 300 kg/m.

The conditions of non-slackened chains and permanently slackened chains were simulated during the tests. A non-slackened chain condition refers to the longwall conveyor's such dynamic condition where no interlink slackening exists in the chain (Dolipski, 1997). This means that the static and dynamic elastic elongation of the chain was compensated by initial tension. In the condition of constant slackening, interlink slackening occurs constantly in the run off point from the drive sprocket drum.

In the case where the condition of constant chain slackening occurred in the tested longwall conveyor, interlink slackening was accumulated in the run off point from the sprocket drum in the auxiliary drive (Fig. 3). For the steady-state motion of the investigated conveyor (in the condition of constant chains' slackening), the maximum dynamic load value in the chain in the place it runs on the sprocket drum in the main drive was $S_{11A}^{H,U\max}$ = 416,2 kN. The sprocket drum in the main drive was loaded with the maximum moment of $M_A^{K,U\max}$ = 195,5 kNm (Fig. 3).

In the case where the elongation of the chain pitch was $\Delta p/p$ = 1%, the maximum value of the force of reaction in the contact point of the rear torus of the horizontal link with the sprocket drum tooth flank in the main drive $F_{11A}^{U\max}$ was 388,5 kN (Fig. 4). On the other hand, the maximum value of the force of reaction between the front torus of the horizontal link and the bottom of the sprocket drum seat in the main drive for the conveyor's steady-state motion $N_{11A}^{U\max}$ was 124,7 kN and the maximum value of the force preventing the slip of the rear torus of the horizontal link at the tooth flank towards the bottom seat (where N = 0) $T_{11A}^{U\max}$ was 17,2 kN.

The value of the chains' initial tension was increased in the next stage of the computer tests (in practise this is done when the longwall conveyor is at standstill). As a result, the elastic elongations of the chain were completely compensated and the condition of non-slackened chains occurred in the conveyor. A higher value of the set initial tension of the chains, in the steady-state motion of the conveyor, increased a dynamic load in the chain in the place where it runs on the sprocket drum in the main drive to $S_{11A}^{H,U\max}$ = 532,6 kN. The maximum load of the drive drum was $M_A^{K,U\max}$ = 195,5 kNm (Fig. 5).

Unauthenticated | 109.197.186.15
Download Date | 10/17/13 8:30 AM

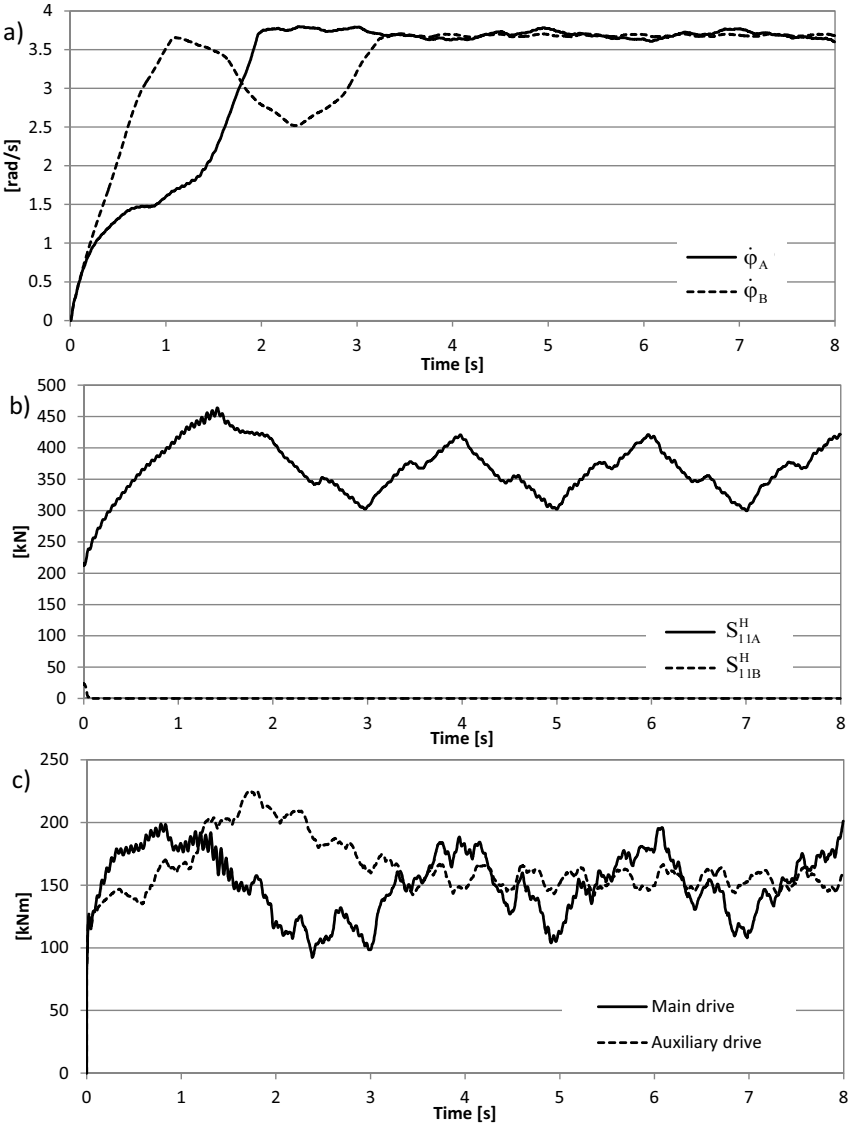

Fig. 3. Start-up and steady-state motion of the longwall scraper conveyor in the condition of constant slackening of chains: a) rotational velocity of sprocket drums, b) dynamic loads in the chain, c) dynamic loads of sprocket drums

The examples of curves for dynamic loads for the sprocket drum teeth and seats in the main drive in the steady-state motion of the investigated longwall conveyor are presented in Fig. 6. In the case where the elongation of the link chain pitch was $\Delta p/p = 1\%$, the maximum values of the loads were: $N_{11A}^{U\max} = 160{,}2$ kN, $F_{11A}^{U\max} = 493{,}2$ kN and $T_{11A}^{U\max} = 22{,}7$ kN.

Unauthenticated | 109.197.186.15
Download Date | 10/17/13 8:30 AM

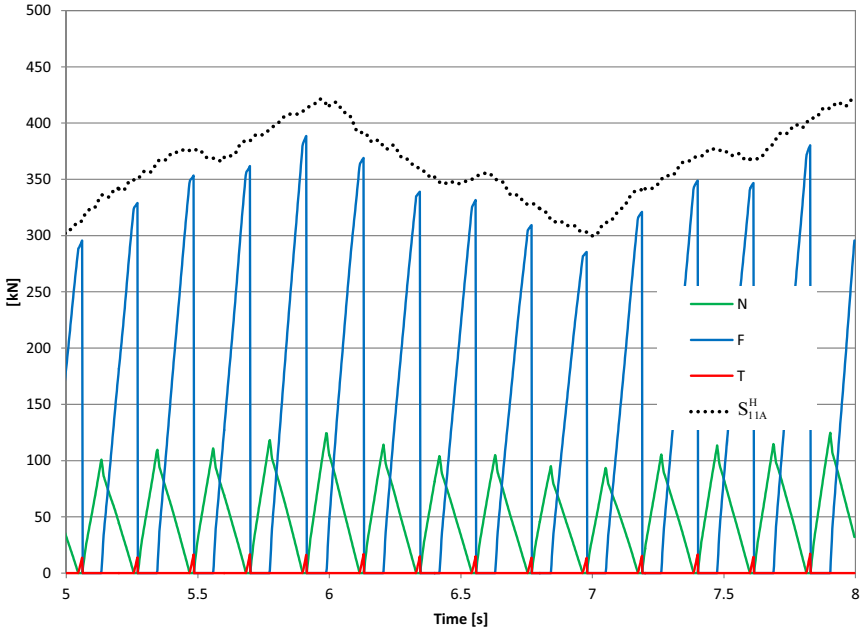

Fig. 4. Dynamic loads of teeth and bottoms of sprocket drum seats in the main drive in the steady-state motion of the conveyor in the condition of constant slackening of chains for the chain pitch elongation of $\Delta p/p = 1\%$

The abrasive wear of the links joints, being the main cause of the higher pitch of the chain links, is decisive for the position of links in the sprocket drum seats, causing the rear torus of the horizontal link to be settled higher and higher on the tooth flank. This shortens the time from the moment the front torus of the horizontal link contacts the seat bottom until the rear torus contacts this link with the tooth flank and extends the time from the moment this reaction reaches a zero value, in the contact point of the front torus of the horizontal link with the seat bottom, until the front torus of the next horizontal link contacts the bottom of the next seat.

An increase in pitch $\Delta p/p$ within the examined range is affecting adversely the maximum value of the force T (it occurs when $N = 0$ and is perpendicular to the reaction F) existing in the steady-state motion of the conveyor. In the condition of a non-slackened chain, its value grew from 22,7 kN to 98,7 kN, and between 17,2 kN to 80,0 kN (Fig. 7) in the condition of constant slackening. It should be emphasised that the increased value of the required friction force at the tooth flank increases the probability of link slip at the tooth flank causing the faster abrasive wear of the teeth and effecting adversely a sprocket wheel's efficiency.

A relationship between the maximum value of the force loading the tooth flank in the contact point of the rear link torus and the maximum value of the force loading the seat bottom in the contact point with the front torus of the link (F/N) is growing nonlinearily as the elongation of the links pitch is growing from 3,1 for pitch growth by 1% to 11,5 for pitch growth by 4%.

As the pitch of the links is growing so is growing the relationship between the maximum value of the required friction force preventing the slip of the rear torus at the tooth flank and the

Unauthenticated | 109.197.186.15
Download Date | 10/17/13 8:30 AM

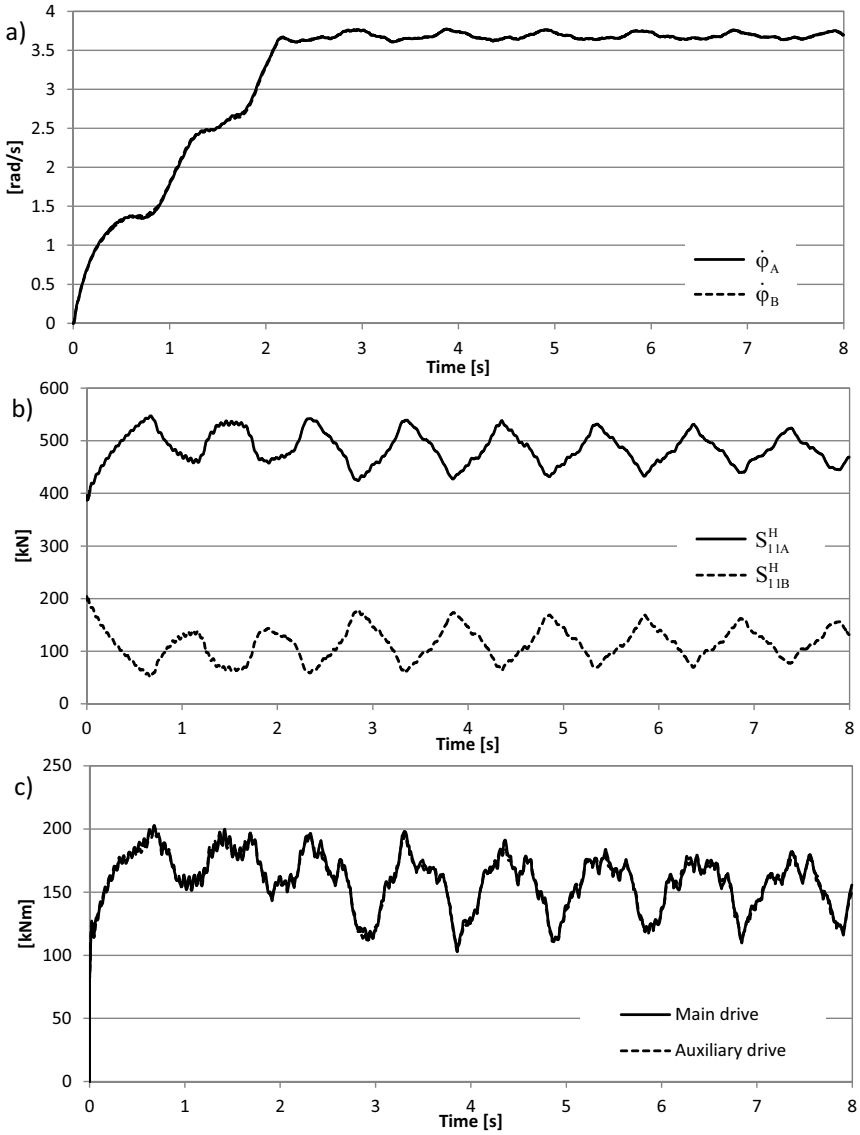

Fig. 5. Start-up and steady-state motion of the longwall scraper conveyor in the condition of non-slackening of chains: a) rotational velocity of sprocket drums, b) dynamic loads in the chain, c) dynamic loads of sprocket drums

maximum value of the force loading the bottom of the seat in the contact point with the front torus of the link (*T*/*N*) from 0,1 for pitch growth by 1% to 2,4 for pitch growth by 4% (Fig. 8). Growth in the relationships of the forces is progressing almost identically for the condition of constant chain slackening and non-slackening.

Unauthenticated | 109.197.186.15
Download Date | 10/17/13 8:30 AM

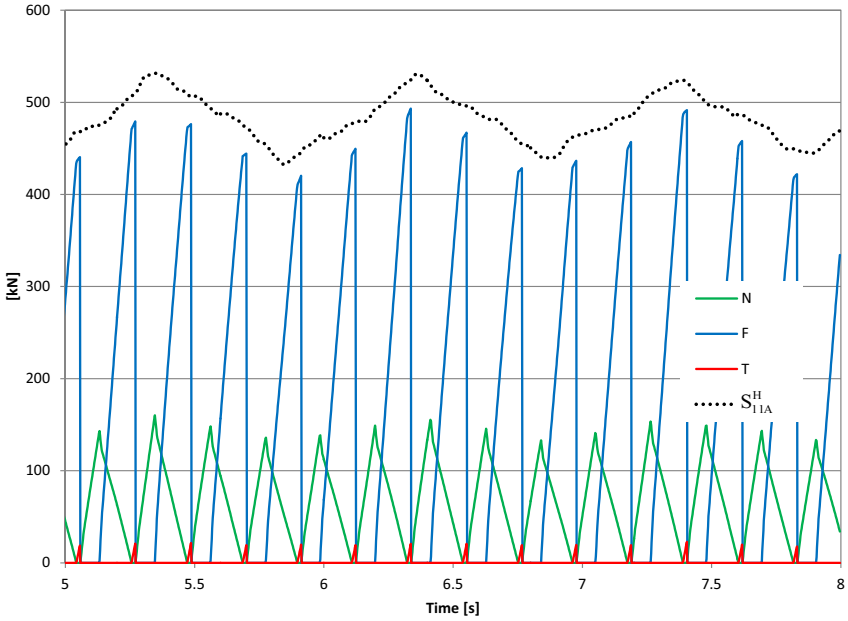

Fig. 6. Dynamic loads of teeth and bottoms of sprocket drum seats in the main drive in the steady-state motion of the conveyor in the condition of constant non-slackening of chains for the chain pitch elongation of $\Delta p/p = 1\%$

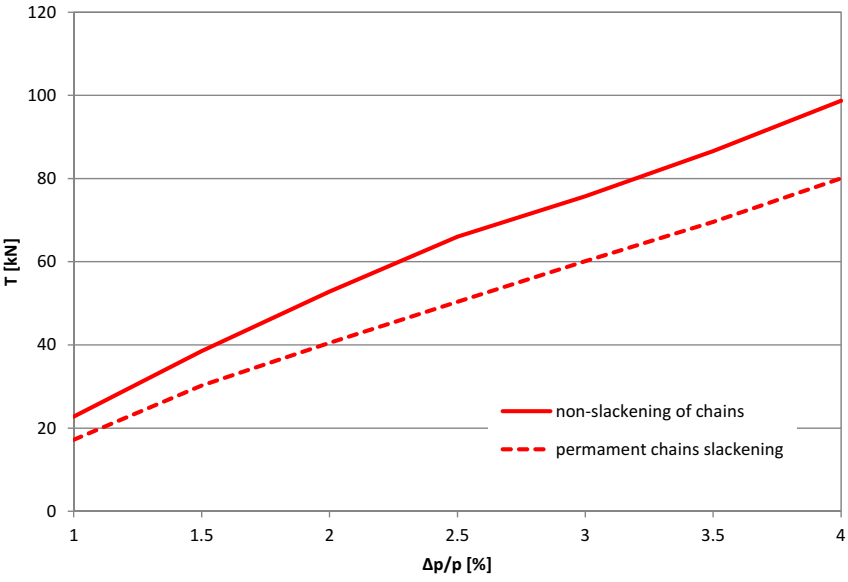

Fig. 7. Impact of the chain pitch elongation $\Delta p/p$ on the maximum value of the friction force T preventing the slip of the rear torus of the horizontal link on the tooth flank towards the seat bottom in the steady-state motion of the longwall conveyor

Unauthenticated | 109.197.186.15
Download Date | 10/17/13 8:30 AM

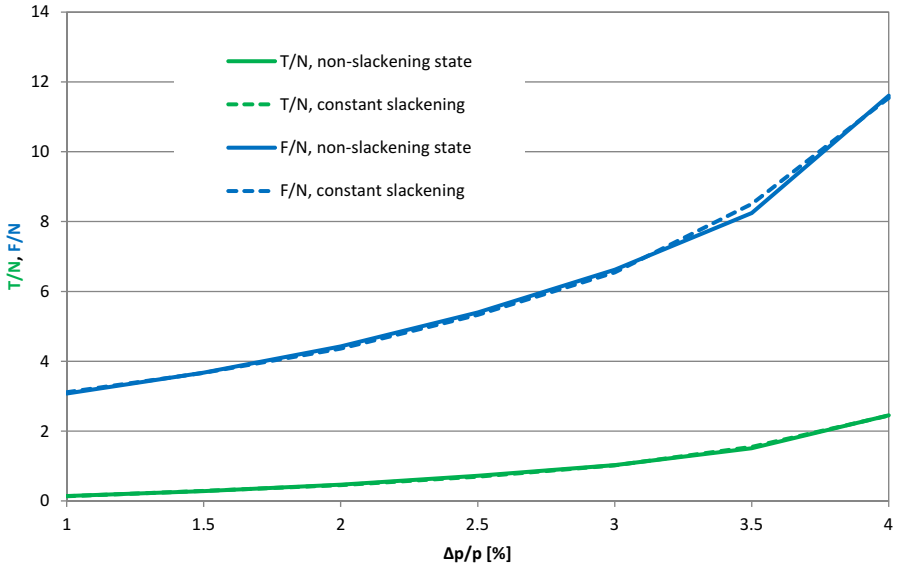

Fig. 8. Impact of the chain pitch elongation $\Delta p/p$ on the relationship between the maximum values of the forces F/N and T/N

4. Summary

An expanded physical and mathematical model of the longwall scraper conveyor allows to determine dynamic loads not only of sprocket drums but also their teeth and seats during start-up and in the steady-state motion. A characteristic feature of a scraper conveyor is the occurrence of high dynamic loads not only during start-up but also for the entire duration of steady-state motion. The following conclusions have been drawn on the basis of the computer tests of the steady-state motion of the longwall scraper conveyor equipped with sprocket drums with the number of teeth $z = 8$, loaded with the mined rock at its entire length:

1. The elongation of the chain pitch, in practise caused mainly by the abrasive wear of the joints links, is causing the rear torus of the horizontal link to settle higher and higher at the tooth flank (higher values of angles ε and α^u). This shortens the time from the moment the front torus of the horizontal link contacts the bottom of the seat until the moment the rear torus of this link contacts the tooth flank. The consequence of this fact is a smaller maximum value of the load on the seat bottom in the contact point with the front torus of the link and a larger maximum value of the required friction force preventing the slip of the rear torus at the tooth flank both, in the condition of constant slackening as well as in the condition of an non-slackened chain.
2. The relationship between the maximum value of the force loading the tooth flank in the contact point with the rear torus of the link and the maximum value of the force loading the seat bottom in the contact point with the front torus of the link and the relationship between the maximum value of the required friction force preventing the slip of the rear torus at the tooth flank to the maximum value loading the seat bottom in the contact point

Unauthenticated | 109.197.186.15
Download Date | 10/17/13 8:30 AM

with the front torus of the link are rising in a non-linear manner as the elongation of the links pitch is growing. Growth in the relationships is progressing almost identically for the condition of constant chain slackening and chain non-slackening.

6. If the chain pitch is increased between 1% to 4%, the maximum value of the friction force preventing the slip of the rear torus of the horizontal link at the tooth flank towards the seat bottom is growing over four times. If the value of the expanded friction force induced by the pressing force of the rear torus of the horizontal link on the tooth flank is at least equal to the value of the considered friction force, then the system of forces is balanced. If, however, the friction force coming from the pressure of the rear torus on the tooth flank is smaller than the value of this friction force, then the slip of the rear torus on the tooth flank towards the seat bottom occurs. For this reason, the high values of the considered friction force in the contact place of the rear torus of the horizontal link with the tooth flank are disadvantageous, as they increase a possibility of link slip occurring on the tooth flank causing the greater abrasive wear of the tooth flank and deteriorating the durability of the sprocket drum and compromising chain meshing efficiency.

The assignment carried out under the development project No. N R09 0026 06/2009 financed by the Ministry of Science and Higher Education under decision No. 0481/R/T02/2009/06

References

Dolipski M., 1997. *Dynamika przenośników łańcuchowych*. Podręcznik akademicki. Wyd. Pol. Śl., Gliwice.

Dolipski M., 2001. *Przeciążenie dynamiczne sprzęgieł podatnych podczas rozruchu przenośnika ścianowego z silnikami dwubiegowymi*. Mechanizacja i Automatyzacja Górnictwa, nr 3.

Dolipski M., Remiorz E., Sobota P., Osadnik J., 2010. *Wpływ zwiększenia podziałki łańcucha na położenie jego ogniw w gniazdach bębnów łańcuchowych*. Wiadomości Górnicze, nr 9.

Hoseinie S. H.; Ataei M., Khalokakaie R., 2011. *Reliability modeling of water system of longwall shearer machine.* Arch. Min. Sci., Vol. 56, No 2.

Kallrath E., Brychta P., 1986. *Strömungskupplungen für schweranlaufende Strebförderer*. Glückauf, nr 12.

Krauze K., Kotwica K., Rączka W., 2009. *Laboratory and underground tests of cutting heads with disc cutters.* Arch. Min. Sci., Vol. 54, No 2.

Krauze K., 2004. *Selection of combined cutter-loader parameters for unidirectional and bidirectional longwall mining systems and the investment costs involved in mining operations.* Arch. Min. Sci., Vol. 49, No 2.

Langosch U., Ruppel U., 2008. *State of the art dimensioning of shield support to optimize longwall roof control*. Arch. Min. Sci., Vol. 53, No 3.

Strümpfel H., 1989. *Zum Antrieb von Ketten mit großer Teilung*. dhf, nr 11

Uhr M., 1993. *Untersuchungen zur Verbesserung des Zusammenwirkens von Kette und Kettenrad*. Glückauf, nr 6

Wölfe M., Flöte K., 2000. *Causes of vibration and stress loadings of chain-operated face equipment resulting from vibration*. Vorträge anläßlich des zweiten internationalen Kolloquiums Hochleistungs-Strebbetriebe. RWTH Aachen, 13-14 Juni.

Ziegler M., Ketting M., Scholten J., 2007. *Dynamische Beanspruchung von Hobel- und Strebförderanlagen*. Glückauf, Nr. 11.

Received: 20 February 2012

Unauthenticated | 109.197.186.15
Download Date | 10/17/13 8:30 AM